A technique for approximating the location of surface- and leaky-wave poles for a lossy dielectric slab

Michael Neve* Robert Paknys†

*University of Auckland, mj.neve@auckland.ac.nz

†Concordia University, robert.paknys@concordia.ca

A Technique for Approximating the Location of Surface- and Leaky-Wave Poles for a Lossy Dielectric Slab

Michael J. Neve, *Member, IEEE,* and Robert Paknys, *Senior Member, IEEE*

***Abstract*—An approximation technique for locating the surface- and leaky-wave poles for a lossy dielectric slab is presented. The problem is reduced to the simultaneous solution of two transcendental equations (for each of the perfect magnetic conductor (PMC) and perfect electric conductor (PEC) cases) which is shown to yield a simple approximate solution for the poles, and which can subsequently be refined using numerical optimization. The technique yields both surface-wave and leaky-wave poles, and results are presented for a typical example to demonstrate the approach. The greatest approximation accuracy was observed for surface-wave and leaky-wave poles well removed from the spectral gap. For poles either within or in close proximity to the spectral gap, an alternative iterative technique is proposed. Expressions for the number of proper plus improper surface-wave poles in a given problem are also derived.**

***Index Terms*—Dielectric waveguides, electromagnetic surface waves, leaky waves.**

I. Introduction

THE lossy concrete slab with an embedded wire structure is of interest to radio system planners deploying broadband wireless communications services in indoor environments. Steel-reinforced concrete is a common building material, and is known to have a significant effect on the transmission of radio signals [1]. Recently, some attention has been focussed on the development of a Green's function/method of moments (GF/MoM) solution for an infinite lossy dielectric slab with a two-dimensional embedded wire matrix [2], [3]. The near field solution to this problem reported in [2], [4] has shown that the presence of an internal wire structure significantly alters the behavior of the transmitted field.

A key requirement in the calculation of the Green's functions for the slab geometry is the location of any relevant surface- and/or leaky-wave poles which are needed when evaluating the contour integral formulation. Techniques for locating the surface- and leaky-wave poles have been considered by a number of authors, e.g., [5, pp. 732–734]–[7]. However, these approaches usually consider the surface- and/or leaky-wave poles separately, or consider only the lossless case. In this paper, we present a technique for rapidly approximating both the surface- and leaky-wave pole locations for the lossy isotropic dielectric slab.

In Section II, the pole equations for the problem considered are presented. Techniques for approximating the surface- and leaky-wave poles for the perfect magnetic conducting (PMC) and perfect electric conducting (PEC) cases are presented in Sections III and IV, respectively. The relationship between the approximation technique and the well-known spectral gap are explored in Section V. The notion of a "split zone" introduced therein is used in Section VI to propose an improvement to the technique for poles which are either deeply within the split zone or for when large-conductivity substrates are being considered. Finally, expressions for the number of proper plus improper surface wave poles in a given problem are derived in Section VII.

II. The Lossy Dielectric Slab

The same terminology used in [2] is employed in this paper. Specifically, a lossy dielectric slab (Region 2) with permittivity ϵ_2 and permeability μ_2 is considered. The surrounding medium (Region 1) is characterized by ϵ_1 and μ_1. An electric line source of strength I_0 is located in Region 1. The wavenumbers k_1 and k_2 for Region 1 and 2, respectively, are defined as $k_1 = \omega\sqrt{\mu_1\epsilon_1}$ and $k_2 = k_1\sqrt{\mu\epsilon}$ where $\mu = (\mu_2/\mu_1)$ and $\epsilon = (\epsilon_2/\epsilon_1)$. We are interested in characterizing the TM_z field in this geometry, and the reader is referred to [2] for further details. Of relevance in this paper is the behavior of the PMC and PEC reflection coefficients, namely

$$\Gamma_m(\eta) = \frac{j\mu\kappa_1 \cot\kappa_2 d + \kappa_2}{j\mu\kappa_1 \cot\kappa_2 d - \kappa_2} \tag{1}$$

and

$$\Gamma_e(\eta) = \frac{j\mu\kappa_1 \tan\kappa_2 d - \kappa_2}{j\mu\kappa_1 \tan\kappa_2 d + \kappa_2}. \tag{2}$$

The parameters κ_1 and κ_2 are given by

$$\kappa_1 = \sqrt{k_1^2 - \eta^2} \tag{3}$$

and

$$\kappa_2 = \sqrt{k_2^2 - \eta^2}. \tag{4}$$

The solution for Γ_m assumes a slab on a PMC ground, whereas Γ_e assumes a slab on a PEC ground. In both cases the slab thickness is d. The presence of Γ_m and Γ_e in the integrand of the Green's function ([2, eq. (4)]) requires the determination of the poles of (1) and (2) prior to performing the contour integration.

Manuscript received October 4, 2004; revised December 13, 2004.

M. J. Neve is with the CSIRO ICT Centre, Epping, NSW 1710, Australia, on leave from the Department of Electrical and Computer Engineering, The University of Auckland, 92019 Auckland, New Zealand (e-mail: m.neve@ieee.org).

R. Paknys is with the Department of Electrical and Computer Engineering, Concordia University, Montreal H3G-1M8, Canada (e-mail: robert.paknys@concordia.ca).

Digital Object Identifier 10.1109/TAP.2005.861530

Expression (3) introduces branch points at $\eta = \pm k_1$ and accordingly the Riemann surface for $\Gamma(\eta)$ has two sheets. To remove these branch points it is convenient to make the substitution [8, pp. 462–464]

$$\eta = k_1 \sin w. \tag{5}$$

The regions where $\mathrm{Re}(w) > 0$, $\mathrm{Im}(w) < 0$ and $\mathrm{Re}(w) < 0$, $\mathrm{Im}(w) > 0$ correspond to values of η on the improper Riemann surface. The poles exhibit an odd symmetry with respect to the origin, but the presence of dielectric loss destroys the pole symmetries about the trajectories $\mathrm{Re}(w) = \pm\pi/2$. The various poles are categorized as either *surface wave* (these can be either proper or improper depending on which Riemann sheet they fall) or *leaky-wave* (which are always improper). Equations (1) (PMC) and (2) (PEC) will each yield a set of poles for any given value of d. It will thus be useful to explore solutions for each of these cases separately.

III. Pole Solutions—PMC Case

We need to determine the values of η for which the denominator of (1) is zero, i.e.

$$j\mu\kappa_1 \cot \kappa_2 d - \kappa_2 = 0. \tag{6}$$

It can be shown that, if $p = \kappa_2 d$ and $q = \kappa_1 d$ then

$$p^2 - q^2 = (\mu\epsilon - 1)(k_1 d)^2 = \ell^2 \tag{7}$$

and

$$p \tan p = j\mu q. \tag{8}$$

Assumming $\mu = 1$, and after some rearrangement of (7) and (8) it can be shown that

$$\begin{aligned} p^2 + p^2 \tan^2 p &= (\epsilon - 1)(k_1 d)^2 = \ell^2 \\ \Rightarrow p \sec p &= \pm\, \ell. \end{aligned} \tag{9}$$

If $p = x + jy$, (9) can be separated into real and imaginary parts, and assuming a lossy material (so that ϵ and therefore ℓ will be complex) then

$$\pm\ell = \pm(l_r + j l_i) = \frac{x + jy}{\cos x \cosh y - j \sin x \sinh y}$$

and so

$$\pm\left[\ell_r \cos x \cosh y + \ell_i \sin x \sinh y\right] - x = 0 \tag{10}$$

and

$$\pm\left[\ell_i \cos x \cosh y - \ell_r \sin x \sinh y\right] - y = 0. \tag{11}$$

Simultaneous solution of (10) and (11) will yield x and y from which p and then η can be determined.

It is useful at this time to plot (10) and (11) in order to visualise the behavior of the desired solution. Unfortunately, these expressions are transcendental in form and are also multivalued. However, a simple way to plot functions of this type is to use a contour plotting package to plot a single contour at height 0. It should be noted from (9) that $p \sec p$ is odd (both real and imaginary parts), and accordingly solutions for p will differ only in sign. As (1) and (2) are not dependent on the sign of p, it is sufficient to only consider the positive solution, namely $p \sec p = +\ell$.

As an example, consider a concrete slab ($\epsilon_r = 6$, $\sigma = 1.95\ \mathrm{mS/m}$) which has a thickness $d = 0.1\ \mathrm{m}$ and an excitation frequency of 1.8 GHz [2]. Corresponding plots of (10) and (11) are given in Fig. 1. The result in Fig. 1 shows

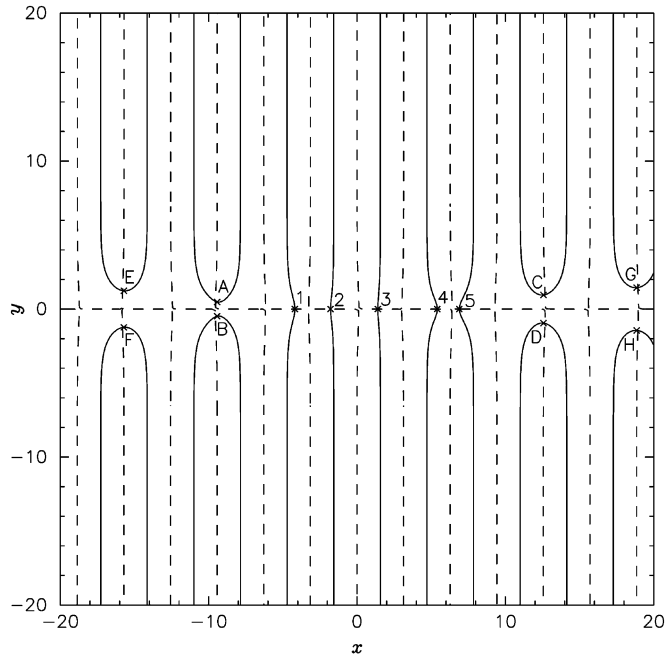

Fig. 1. Plots of (10) (solid line) and (11) (dashed line) for the PMC case. The solutions labeled $(1 \ldots 5)$ and $(A \ldots H)$ correspond to the surface- and leaky-wave poles, respectively, in Fig. 2.

solutions of two different types, namely (a) a finite number of solutions (labeled $1 \ldots 5$) for (10) where $y \simeq 0$; and (b) complex solutions (labeled $A \ldots H$) for (10) separated by multiples of 2π, namely $x \simeq (4\pi, 6\pi, 8\pi, \ldots)$ for $x > 0$ and $x \simeq (-3\pi, -5\pi, -7\pi, \ldots)$ for $x < 0$. This is a very useful observation, since these approximations for x are integer multiples of π and are not dependent on the physical geometry, material properties or frequency. Furthermore, this result suggests that solutions (a) correspond to the surface wave poles and (b) to leaky-wave poles. To test this hypothesis it will be useful to consider separate solutions in each of these regimes.

A. PMC Case—Surface-Wave Poles

Fig. 1 suggests that $y \simeq 0$ for the surface-wave poles. The approximate location for the surface-wave poles can be found by substituting $y = 0$ in (10). Accordingly

$$\begin{aligned} x &= \pm\, \ell_r \cos x \\ \Rightarrow \ell_r \cos x - x &= 0 \end{aligned} \tag{12}$$

where the $\pm$ has been dropped for the reason outlined previously. Estimates for x can be determined using a simple root finding algorithm. Given the predictable oscillatory nature of (12), a bracketing approach (such as bisection) is well suited to this role. Once these estimates have been obtained, using (4) it can be shown that

$$\eta = \pm\sqrt{k_2^2 - \left(\frac{x}{d}\right)^2}.$$

The question now arises as to which of the two possible Riemann sheets correspond to the solutions for η which produce poles. To determine the correct nature of these poles it is necessary to calculate $\Gamma_m(\eta)$ using (1) for both the proper $\mathrm{Im}(\kappa_1) < 0$ and improper $\mathrm{Im}(\kappa_1) > 0$ Riemann sheets. This procedure will only yield a "large" value for Γ_m on either the proper or improper Riemann sheets, *but not both*.

TABLE I
ESTIMATES OF x, y, APPROXIMATIONS FOR w, AN OPTIMISED ESTIMATE w' AND $|w - w'|$ FOR THE PMC EXAMPLE

Pole	x	y	w	w'	$\lvert w - w' \rvert$
1	-4.19	0.0	$1.57 + j1.42$	$1.57 + j1.41$	6.82×10^{-5}
2	-1.78	0.0	$1.57 - j1.52$	$1.57 - j1.52$	1.14×10^{-5}
3	1.40	0.0	$1.57 + j1.53$	$1.57 + j1.53$	5.42×10^{-6}
4	5.40	0.0	$1.57 - j1.31$	$1.57 - j1.31$	2.15×10^{-4}
5	6.90	0.0	$1.58 + j1.07$	$1.57 + j1.07$	5.29×10^{-4}
A	-9.42	0.48	$2.75 - j0.67$	$2.70 - j0.61$	8.11×10^{-2}
B	-9.42	-0.48	$0.40 - j0.68$	$0.46 - j0.62$	8.47×10^{-2}
C	12.57	0.95	$0.15 - j1.57$	$0.15 - j1.55$	1.64×10^{-2}
D	12.57	-0.95	$3.00 - j1.57$	$2.99 - j1.55$	1.56×10^{-2}
E	-15.71	1.23	$3.03 - j1.94$	$3.03 - j1.93$	8.42×10^{-3}
F	-15.71	-1.23	$0.11 - j1.94$	$0.12 - j1.93$	8.84×10^{-3}
G	18.85	1.44	$0.098 - j2.18$	$0.099 - j2.18$	5.95×10^{-3}
H	18.85	-1.44	$3.04 - j2.18$	$3.04 - j2.18$	5.66×10^{-3}

Once the correct sheet has been identified, an estimate for w can be made. Given the mapping operation (5), we can calculate w from

$$w = \sin^{-1}\left(\frac{\eta}{k_1}\right).$$

If the pole has $\mathrm{Im}(\kappa_1) < 0$ and is located on the improper Riemann sheet, *or* the pole has $\mathrm{Im}(\kappa_1) > 0$ and is located on the proper Riemann sheet, then w should be replaced by[1]

$$w = -w + \pi$$

thereby forcing the pole to lie in the correct location in the w-plane.

It must be noted that the values for w thus calculated are only approximations to the solution of (10) and (11). A much closer estimate of the pole locations can be obtained if multidimensional optimization is adopted using the approximate values calculated above as seeds. Estimates of x, y, approximations for w, an optimized estimate w' and the approximation error $|w - w'|$ for the example being considered are listed in Table I. These approximate and optimized estimates for w are also shown in Fig. 2. The location of the poles labeled $(1 \ldots 5)$ confirms the hypothesis that these poles are indeed surface-wave poles.

B. PMC Case—Leaky-Wave Poles

A similar approach can be taken for the leaky-wave poles, by noting from Fig. 1 that complex solutions for (10) exhibit the same geometrical/material/frequency independent properties as the surface-wave poles in Section III-A. For the leaky-wave poles, the complex solutions are separated by approximately 2π and are located at $x \simeq (4\pi, 6\pi, 8\pi, \ldots)$ for $x > 0$, and $x \simeq (-3\pi, -5\pi, -7\pi, \ldots)$ for $x < 0$. Given this behavior, it is possible to rewrite (10) as

$$y = \cosh^{-1}\left(\frac{|x|}{\ell_r}\right).$$

The corresponding values of η and w can now be calculated, given that these poles must all by definition be located on the improper Riemann sheet. As with the surface-wave poles, the values for w thus calculated can be improved using multidimensional optimization. Estimates of x, y, approximations for w, an optimized estimate w' and the approximation error $|w - w'|$ for the example being considered are also listed in Table I, and illustrated in Fig. 2.

It is interesting to note that the greatest accuracy is achieved for the surface-wave poles. This is useful since it is the proper subset of these poles (in this example numbered (in order) 3, 1 and 5) that are first "encountered" by the steepest descent integration contour used to evaluate the Green's function [2]. The accuracy achieved suggests that the approximation technique may well be sufficient in the determination of these poles and that further optimization may not be necessary. It can also be seen that the accuracy of the leaky-wave pole approximations improve as $|\mathrm{Im}(w)|$ increases. The least accuracy is obtained in the region where $\mathrm{Im}(w)$ is small negative and this behavior is discussed further in Section VI.

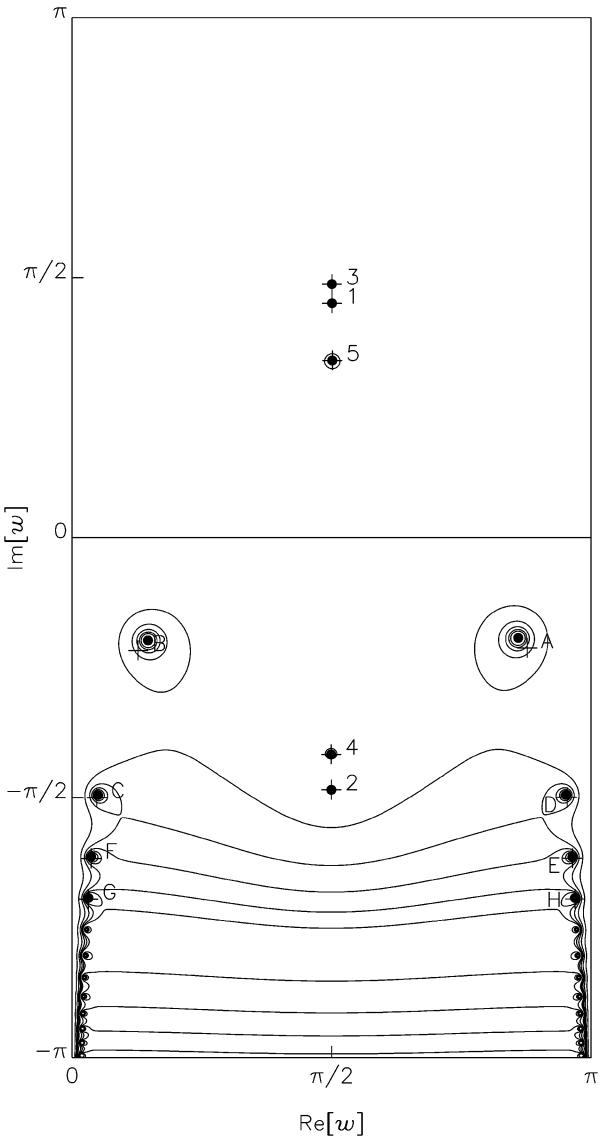

Fig. 2. Plot of the w-plane for example showing locations of three proper surface-wave poles (1, 3, 5), two improper surface-wave poles (2, 4) and the first eight leaky-wave poles $(A \ldots H)$ for the PMC case. (The initial approximations to the poles are shown by the "+" symbols, and the optimized estimates by the "•" symbols).

[1]According to the definition $\arcsin z = (-1)^k \arcsin z + k\pi$ where k is an arbitrary integer [9, p. 80].

IV. Pole Solutions—PEC Case

In a manner similar to the PMC case, we need to determine the values of η for which the denominator of (2) is zero, i.e.

$$j\mu\kappa_1 \tan\kappa_2 d + \kappa_2 = 0.$$

Given the same definitions for p and q as in Section III and the PEC "dual" of (8) namely

$$-p\cot p = j\mu q \tag{13}$$

rearrangement of (7) and (13) with $\mu = 1$ yields

$$p^2 + p^2\cot^2 p = (\epsilon - 1)(k_1 d)^2 = \ell^2$$
$$\Rightarrow p\csc p = \pm\,\ell. \tag{14}$$

It should be noted that the lossless case has already been considered by Collin [5, pp 732–734]. However, here we are interested in the lossy case, so defining $p = x + jy$, we can separate (14) into real and imaginary parts, and assuming a lossy material (so that ϵ and therefore ℓ will be complex) then

$$\pm\ell = \pm(l_r + jl_i) = \frac{-j(x+jy)}{\cos x\sinh y - j\sin x\cosh y}$$

and so

$$\pm\left[\ell_r\cos x\sinh y + \ell_i\sin x\cosh y\right] - y = 0 \tag{15}$$
$$\mp\left[\ell_i\cos x\sinh y - \ell_r\sin x\cosh y\right] - x = 0. \tag{16}$$

Simultaneous solution of (15) and (16) will yield x and y from which p and then η can be determined.

A similar approach as used in Section III has been adopted in the PEC case. However, unlike the PMC case in Section III it is not possible in the PEC case to ignore the two solutions given by the different signs in (15) and (16). Each of these contribute poles to the final solution, and hence their separate consideration is necessary. Accordingly, in Case I we seek the solution of

$$\left[\ell_i\cos x\sinh y - \ell_r\sin x\cosh y\right] - x = 0 \tag{17}$$

and

$$\left[\ell_r\cos x\sinh y + \ell_i\sin x\cosh y\right] + y = 0 \tag{18}$$

whereas in Case II we seek the solution of

$$\left[\ell_i\cos x\sinh y - \ell_r\sin x\cosh y\right] + x = 0 \tag{19}$$

and

$$\left[\ell_r\cos x\sinh y + \ell_i\sin x\cosh y\right] - y = 0. \tag{20}$$

Plots of (17), (18) (Case I) and (19), (20) (Case II) are similar in form to that obtained for the PMC case.

A. PEC Case—Surface-Wave Poles

As in the PMC case, the approximate location of the surface-wave poles can be found by setting $y = 0$. However, we need to consider Case I and Case II separately which yield, from (17) and (19), respectively, the two equations

$$\text{Case I}: x = -\,l_r\sin x \tag{21}$$
$$\text{Case II}: x = l_r\sin x. \tag{22}$$

The solution $x = y = 0$ (ie $\kappa_2 = 0$) for both Cases I and II need not be considered further, as it can be shown using L'Hopital's rule that the magnitude of (2) remains finite in this case. The remaining part of the procedure (including checking the Riemann sheets) is virtually identical to that for the PMC surface-wave poles.

B. PEC Case—Leaky-Wave Poles

A similar approach can be taken as for the PMC leaky-wave poles, except that Cases I and II need to be considered separately. In Case I, complex solutions for (17) and (18) are seen to occur for $x \simeq \pm 3\pi/2, \pm 7\pi/2, \pm 11\pi/2\ldots$ which can be substituted into (17) to give

$$y = \cosh^{-1}\left(\frac{x}{l_r}\right). \tag{23}$$

Similarly, in Case II, complex solutions for (19) and (20) are seen to occur for $x \simeq \pm 5\pi/2, \pm 9\pi/2, \pm 13\pi/2\ldots$ which can be substituted into (19) to give the same result as (23). As with the PMC poles improved poles estimates can be obtained if multidimensional optimization is adopted using the approximate values as seeds.

V. Pole Approximations and the Spectral-Gap

The approach presented in Sections III and IV has been shown to yield estimates of both the surface-and leaky-wave pole locations. Of interest is the behavior of the leaky-wave pole "loops," arising due to (10) in Fig. 1 for the PMC case, and (17) and (19) for the PEC case. These "loops" (the stationary points of which approximate the leaky-wave pole solutions) are seen to vertically converge and join to give solutions that correspond to the surface-wave pole solutions, as the excitation frequency increases. This transitional behavior is consistent with the observations reported in [10]–[12] concerning the spectral-gap region in which a physically meaningful leaky mode transitions to a bound surface-wave mode. In the case of lossless substrates, the spectral-gap behavior is characterized by a split point at which the leaky-wave poles merge to form a double pole, and then separate to ultimately become a proper/improper surface-wave pole pair. Such a split point does not occur for lossy substrates, but it is useful to introduce the qualitative notion of a "split zone" as the nominal region where the leaky-wave poles pass closest to each other.

VI. Improvements

The approximation technique described in Sections III and IV has been shown to yield the greatest accuracy for poles well removed from the split zone. In general, multidimensional numerical optimization can subsequently be used to refine these initial approximations (if required). Conversely, the least accurate initial approximations were obtained when the poles of interest were either within or in close proximity to the split zone—for example, poles "A" and "B" in Fig. 2 and Table I. The initial approximations in this case were still sufficiently accurate to function as valid seeds for the numerical optimizer. However, when considering poles located deep within the split zone, the initial approximations might well prove unreliable for use as seeds. The approximation technique proposed is fundamentally dependent on the specific nature of (11) (PMC) and (18), (20) (PEC) which (in the case of low-loss substrates) exhibit gradients which are either very large or virtually zero. It is this characteristic that makes the approximation of the intersections [and thereby the solutions to the simultaneous equation pairs (10)/(11) (PMC) and (15)/(16) (PEC)] almost trivial. It has also

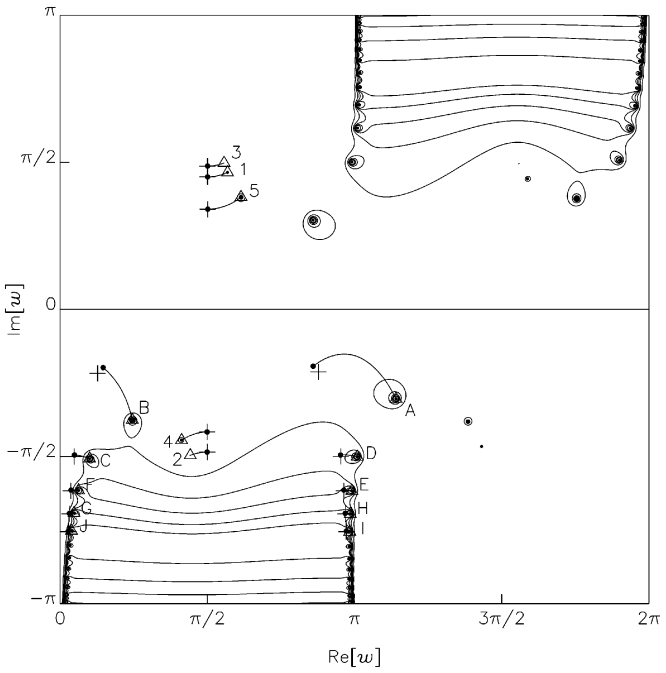

Fig. 3. Plot of w-plane for "large" conductivity example showing locations of five surface-wave poles $(1 \ldots 5)$ and the first ten leaky-wave poles $(A \ldots J)$ for the PMC case. (The initial "small" conductivity approximations to the poles are shown by the "+" symbols, the "small" conductivity optimized estimates by the "•" symbols, and the final "large" conductivity optimized estimates by the "△" symbols).

been observed that large substrate conductivities can cause sufficient distortion in the results plotted in Fig. 1 so as to invalidate these assumptions.

Fortunately, a simple approach can be used to circumvent these difficulties. The key idea behind this approach is to derive approximate solutions (using the method described in Sections III and IV) in a region where the poles of interest are both well removed from the split zone and for substrate conductivities that are not excessive. These approximations can then be tracked toward the solution of interest using estimates calculated at each iteration to seed the next iteration step. Practically, this means commencing the procedure at a sufficiently low frequency such that all poles are leaky, and then gradually increase the frequency tracking the poles until the desired value is obtained. In the case of high-conductivity substrates the equivalent procedure would be to start with a low substrate conductivity for which the approximation is valid and then track the poles to the final desired conductivity. These procedures can of course be combined.

To illustrate this approach, consider the example in Fig. 2 but for a "large" conductivity $\sigma = 0.2\ \mathrm{S/m}$. As shown in Fig. 3, the approximation technique is used to derive initial estimates for a conductivity $\sigma = 2\ \mathrm{mS/m}$ as shown by the "+" symbols. These were then optimized to yield the estimates shown as the "•" symbols. The conductivity of the substrate was then progressively incremented and each pole estimate thus obtained used to seed the subsequent iteration until the desired conductivity was achieved (the final estimates for $\sigma = 0.2\ \mathrm{S/m}$ are shown as the "△" symbols). In this example the initial approximations to the poles were sufficiently good so as to not require frequency stepping, but this could easily have been performed prior to the conductivity stepping.

It must be kept in mind that this tracking procedure will not work in the lossless case in which each pair of leaky-wave poles merge at the split point to become a double pole, then split to form a pair of improper surface-wave poles and ultimately a proper/improper surface-wave pole pair as described in [11]. In this case iterating with respect to frequency can still be used but starting at a higher frequency and then decrementing is required.

VII. Pole Approximations and the Split Zone

The nominal center of the split zone for a given pole pair occurs whenever the corresponding leaky-wave pole "loops" in Fig. 1 touch in the vicinity of $y \simeq 0$. At this point, expressions (12) (PMC case) and (21), (22) (PEC Cases I and II, respectively) apply. In both cases, the split zone is defined by the problem geometry and we thus need to determine the discrete set of values that l_r can take with each value corresponding to the "split" of a pair of leaky-wave poles. In the PMC case, this is done by noting from Fig. 1 that the split points occur when the linear and cosine terms in (12) are tangential. Accordingly, x can be approximated by equating the first derivatives of the left- and right-hand sides of (12) and then substituting the result in (12) to give

$$\sin^{-1}\left(\frac{1}{l_r}\right) - n_m\pi + \sqrt{l_r^2 - 1} = 0, \quad n_m = 1, 2, 3 \ldots. \tag{24}$$

A similar approach can be taken for the PEC case yielding

$$\cos^{-1}\left(\frac{1}{l_r}\right) + n_e^I\pi - \sqrt{l_r^2 - 1} = 0, \qquad n_e^I = 1, 3, 5 \ldots \text{ (Case I)}$$

$$\cos^{-1}\left(\frac{1}{l_r}\right) + n_e^{II}\pi - \sqrt{l_r^2 - 1} = 0, \qquad n_e^{II} = 2, 4, 6 \ldots \text{ (Case II)}$$

or in general

$$\cos^{-1}\left(\frac{1}{l_r}\right) + n_e\pi - \sqrt{l_r^2 - 1} = 0, \quad n_e = 1, 2, 3 \ldots. \tag{25}$$

Expressions (24) and (25) can be used to approximate the set of values for l_r which correspond to the nominal split-zone center. These can then be used to decide whether the approximations derived using the technique in Sections III and IV can be either used directly or after optimization, or whether the iterative approach described in Section VI is necessary.

Alternatively, if l_r is known, these expressions can be solved for n_m and n_e (assumed real) and thus used to determine how many leaky-wave poles have transitioned through the split zone and become surface-wave poles. It should be noted that these expressions only consider the tangent behavior and give no valid solution for $l_r < 1$. However, in the PMC case there is at least one surface-wave pole due to the intersection of the linear and $\cos(\cdot)$ term in (12). The first "split" occurs when the linear and and $\cos(\cdot)$ term in (12) are tangential (corresponding to $n_m = 1$). As each leaky-wave "loop" in Fig. 1 gives rise to two surface-wave poles, the number of surface-wave poles arising from the PMC solution can be written as

$$N_m = \begin{cases} 1 & l_r < 1 \\ 2\lfloor n_m \rfloor + 1 & l_r \geq 1 \end{cases}$$

where $\lfloor n_m \rfloor$ is the largest integer smaller than or equal to n_m. Similarly, in the PEC case there are no surface-wave poles for $l_r < 1$, and for $l_r \geq 1$ there is only one pole until the linear and $-\sin(\cdot)$ terms are tangential in (21) (corresponding to $n_e^I = 1$). Accordingly, the number of surface-wave poles arising from the PEC solution is given by

$$N_e = \begin{cases} 0 & l_r < 1 \\ 2\lfloor n_e \rfloor + 1 & l_r \geq 1 \end{cases}$$

in which the number of poles determined for Cases I and II have been combined.

VIII. Conclusion

An approximate technique for locating both the surface-wave and leaky-wave poles for a lossy dielectric slab has been presented. Both PMC and PEC cases have been considered, with both yielding pole solutions that arise from the simultaneous solution of two transcendental equations. Although transcendental in form, in both cases a simple approximate solution for the poles has been derived. The result obtained is very useful since it is yields approximate solutions which are not dependent on the physical geometry, material properties or frequency. In the example considered, the greatest prediction accuracy was observed for surface-wave poles and for leaky-wave poles well removed from the split zone. Multidimensional numerical optimization can be used to refine the pole estimates.

For poles located deep within the split zone or for substrates with large conductivity, the approximation accuracy decreases and the estimates thus obtained may be unsuitable for use as seeds in optimization. For these cases an alternative approach has been proposed which uses estimates from the approximation technique applied in a "stable" location (removed from split zone), which are then iterated toward the desired solution. An example of a substrate with a large conductivity has been considered to illustrate this procedure.

The behavior of the approximate solutions in the vicinity of the split zone was also investigated and used to derive expressions for the number of proper plus improper surface-wave poles in a given problem.

Acknowledgment

The authors wish to thank the reviewers for their valuable and useful comments.

References

[1] S. Y. Seidel and T. S. Rappaport, "914 MHz path loss prediction models for indoor wireless communications in multifloored buildings," *IEEE Trans. Antennas Propag.*, vol. AP-40, pp. 207–217, 1992.

[2] R. Paknys, "Reflection and transmission by reinforced concrete—Numerical and asymptotic analysis," *IEEE Trans. Antennas Propag.*, vol. AP-51, pp. 2852–2861, Oct. 2003.

[3] R. Paknys, M. J. Neve, and A. G. Williamson, "Theory and experiment for UHF propagation through reinforced concrete," in *Proc. IEEE APS/URSI Int. Symp.*, Montreal, Canada, Jul. 13–18, 1997, pp. 442–442.

[4] M. J. Neve, A. G. Williamson, and R. Paknys, "Propagation modeling of composite inhomogeneous materials for in-building wireless systems," in *Proc. IEEE APS/URSI Int. Symp.*, Monterey, Jun. 20–26, 2004.

[5] R. E. Collin, *Field Theory of Guided Waves*, 2nd ed. New York: IEEE Press, 1991.

[6] M. A. Marin, S. Barkeshli, and P. H. Pathak, "On the location of proper and improper surface wave poles for the grounded dielectric slab," *IEEE Trans. Antennas Propag.*, vol. AP-38, pp. 570–573, Apr. 1990.

[7] C.-I. G. Hsu, R. F. Harrington, J. R. Mautz, and T. K. Sarkar, "On the location of leaky wave poles for a grounded dielectric slab," *IEEE Trans. Microwave Theory Tech.*, vol. MTT-39, pp. 346–349, Feb. 1991.

[8] L. B. Felsen and N. Marcuvitz, *Radiation and Scattering of Waves*, 1st ed, NJ: Prentice Hall, 1973.

[9] M. Abramowitz and I. Stegun, *Handbook of Mathematical Functions*, 5th ed. New York: Dover, 1968.

[10] P. Lampariello, F. Frezza, and A. A. Oliner, "The transition region between bound-wave and leaky-wave ranges for a partially dielectric-loaded open guiding structure," *IEEE Trans. Microwave Theory Tech.*, vol. MTT-38, pp. 1831–1836, Dec. 1990.

[11] S. Majumder, D. R. Jackson, A. A. Oliner, and M. Guglielmi, "The nature of the spectral gap for leaky waves on a periodic strip-grating structure," *IEEE Trans. Microwave Theory Tech.*, vol. MTT-45, pp. 2296–2307, Dec. 1997.

[12] P. Y. Ufimtsev, R. T. Ling, and J. D. Scholler, "Transformation of surface waves in homogeneous absorbing layers," *IEEE Trans. Antennas Propag.*, vol. 48, pp. 214–222, Feb. 2000.

Michael J. Neve (S'87–M'91) was born in Auckland, New Zealand on October 29, 1966. He received the B.E.(Hons) and the Ph.D. degrees from the University of Auckland in 1988 and 1993, respectively.

From May 1993 to May 1994, he was a Leverhulme Visiting Fellow at the University of Birmingham, Birmingham, U.K. During this time, he was involved with radiowave propagation research using scaled environmental models. From May 1994 to May 1996, he was a New Zealand Science and Technology Postdoctoral Fellow within the Department of Electrical and Electronic Engineering at the University of Auckland. From May 1996 to December 2000, he was a part-time Lecturer/Senior Research Engineer in the Department of Electrical and Electronic Engineering at the University of Auckland. In 2004, he was a Visiting Scientist at the CSIRO ICT Centre in Sydney, Australia and is presently a Senior Lecturer and Graduate Advisor in the Department of Electrical and Computer Engineering at the University of Auckland. His present research interests include radiowave propagation modeling in cellular/microcellular/indoor environments, the interaction of electromagnetic fields with man-made structures, cellular system performance optimization and antennas.

He was jointly awarded a 1992/1993 Institution of Electrical Engineers (IEE) Electronics Letters Premium for two publications resulting from his doctoral research. He is currently Vice Chair of the IEEE New Zealand North Section.

Robert Paknys (S'78–M'85–SM'97) was born in Montreal, QC, Canada, on June 29, 1956. He received the B.Eng. degree from McGill University, Montreal, QC, Canada, in 1979 and the M.Sc. and Ph.D. degrees from The Ohio State University, Columbus, in 1982 and 1985, respectively, all in electrical engineering.

From 1980 to 1985, he was a Graduate Research Assistant with the ElectroScience Laboratory, Ohio State University. During 1985 to 1987, he was an Assistant Professor with the Department of Electrical and Computer Engineering, Clarkson University, Potsdam, NY. During 1987 to 1989, he was an Engineer with the Electromagnetics Division of MPB Technologies, Incorporated, Dorval, QC, Canada. Since 1989, he has been a faculty member with the Department of Electrical and Computer Engineering, Concordia University, Montreal, and during 1996 to 2001, he served as the Undergraduate Program Director. In 1996, he was an Honorary Research Fellow at the ECE Department, University of Auckland, New Zealand. In 2004 he was a Visiting Research Associate Professor at the ECE Department, University of Houston, TX. He has acted as a Consultant for MPB Technologies Incorporated, Canadian Astronautics Ltd., Infield Scientific Incorporated, SNC Technologies Incorporated, and Defense Research and Development Canada. His research interests are in computational electromagnetics and high frequency asymptotic methods, with applications to antennas, propagation, scattering, and diffraction.

Dr. Paknys is a Registered Professional Engineer, with the Order of Engineers of Quebec. He is a Member of the Applied Computational Electromagnetics Society (ACES). He is a licensed radio amateur, with callsign VE2JBP. He is presently an Associate Editor for the IEEE Transactions on Antennas and Propagation.